JOURNAL OF SOLID STATE CHEMISTRY 108, 236–242 (1994)

Microstructural Characterization of the Fluorite Phase in the U–La–O System

II. Hexagonal Microdomain Formation in $(U_{1-y}La_y)O_{2-x}$, $0.70 \leq y \leq 0.80$

P. Garcia-Chain, R. M. Rojas[1], P. Herrero, and J. R. Günter*

*Instituto de Ciencia de Materiales de Madrid, C.S.I.C., Serrano 113, 28006 Madrid, Spain; and *Institute for Inorganic Chemistry, Winterthurerstrasse 190, CH-8057 Zürich, Switzerland*

Received February 22, 1993; Accepted May 25, 1993

Fluorite-type materials $(U_{1-y}La_y)O_{2-x}$ within the compositional range $0.70 \leq y \leq 0.80$ have been characterized by X-ray diffraction and transmission electron microscopy. Their microstructures are discussed in terms of microdomain formation of a secondary phase, denominated R_{II}, coherently intergrown with the fluorite matrix. Annealing of the materials $y = 0.73$ and $y = 0.74$ at 1100°C for 500 hr leads to the formation of the R_{II} phase as a single phase, which may be described as a superstructure $\sqrt{2}a_c \times \sqrt{2}a_c \times \sqrt{3}a_c$ of the fluorite cell. A new set of lattice parameters has been determined on the basis of a primitive trigonal cell, being $a_h = 0.78220(4)$ nm and $c_h = 0.99712(7)$ nm for the composition $y = 0.74$. Relationships between the fluorite and the R_{II} cells are presented.

INTRODUCTION

Certain kinds of metal atoms M are known to substitute for uranium atoms in UO_2 forming solid solutions $(U_{1-y}M_y)O_{2\pm x}$, $(x \geq 0)$ under suitable conditions. Depending both on the valency of such M metals, which are in the range between 4^+ and 2^+ and on the experimental conditions, the oxidation state of uranium can change considerably. Consequently the overall oxygen/metal ratio varies, giving rise to nonstoichiometric mixed oxides. Because of the high yields of some rare-earth and alkaline-earth metals during fission reactions, the solid solutions between urania and most of these metals have been studied extensively (1–8). Moreover, it has been shown that urania-based nonstoichiometric mixed oxides with M = Sc, Y, Pr, Dy, are good electrode materials particularly suitable for oxygen sensors and offer some advantages over conventional noble metals (9).

Most of these compounds formed at high temperatures crystallize in the fluorite-type structure. Structural and microstructural studies carried out on some of these systems and other related ones have revealed the complexity of these materials in which the description of nonstoichiometric phases in terms of a random distribution of point defects is no longer adequate. Instead, they have to be more accurately described as microheterogeneous in character, that is, as fluctuating systems which consist either of microdomains differing in structure and/or composition from the parent matrix but dispersed in a coherent way with it (10–13), or as a continuous and commensurate modulation of the fluorite-type structure (14–16).

Within this scope, a reinvestigation of the phases formed in the pseudobinary UO_2–$LaO_{1.5}$ is currently being carried out. The phase diagram for this system indicates the formation of a fluorite phase (space group $Fm3m$) in the composition range $(U_{1-y}La_y)O_{2\pm x}$, $0.26 \leq y \leq 0.80$ at high temperatures. Moreover, the existence of three ordered phases R_I, R_{II}, and R_{III} at lower temperature has been pointed out (17, 18). In previous papers, evidence of R_{III} rhombohedral microdomains formation at 1400°C, in the composition range $0.56 \leq y \leq 0.67$, has been stated (12, 19).

The purpose of this paper is to present results of combined transmission electron microscopy (TEM) and X-ray diffraction studies carried out in the $0.70 \leq y \leq 0.80$ range, in which the existence of the ordered rhombohedral R_{II} phase at temperature below 1300°C has been reported. This phase was first described by Diehl and Keller (17), and only X-ray powder diffraction data are available. It has been indexed on the basis of a hexagonal–rhombohedral cell, that is, a rhombohedral symmetry in hexagonal setting, with parameters $a_h = 1.036$ nm and $c_h = 0.9987$ nm (17, 18). The phase $U_2Sm_6O_{15}$ formed in the UO_2–UO_3–Sm_2O_3 system is so far the only one that has been pointed out to have the R_{II} structure (20).

EXPERIMENTAL

Samples within the compositional range $(U_{1-y}La_y)O_{2\pm x}$, $0.70 \leq y \leq 0.80$ were prepared by a mixed ceramic/organic

[1] To whom correspondence should be addressed.

0022-4596/94 $6.00

TABLE 1
Lanthanum Content (y), Synthesis and Annealing Conditions and Obtained Phases for $(U_{1-y}La_y)O_{2-x}$ Materials

y	Synthesis	Obtained phases	Annealing	Obtained phases
0.70	1400°C/150 hr	F	1100°C/500 hr	F + R_{II}
0.72	1400°C/150 hr	F	1100°C/500 hr	F + R_{II}
0.73	1400°C/150 hr	F	1100°C/500 hr	R_{II}
	1100°C/700 hr	R_{II}		
0.74	1400°C/150 hr	F	1100°C/500 hr	R_I
	1100°C/700 hr	R_{II}		
0.75	1400°C/150 hr	F	1100°C/500 hr	F + R_{II}
0.80	1400°C/150 hr	F	1100°C/500 hr	F + R_{II}

Note. F: Fluorite type structure; R_{II}: Hexagonal structure.

TABLE 2
Lanthanum Content (y), Experimental Composition and Cell Parameter Values for $(U_{1-y}La_y)O_{2-x}$ Fluorite-type Materials

y	Composition	a (nm)
0.70	$U_{0.30}La_{0.70}O_{1.95}$	0.55852(2)
0.72	$U_{0.28}La_{0.72}O_{1.92}$	0.56003(2)
0.73	$U_{0.27}La_{0.73}O_{1.90}$	0.56034(2)
0.74	$U_{0.26}La_{0.74}O_{1.89}$	0.56069(2)
0.75	$U_{0.25}La_{0.75}O_{1.87}$	0.56093(3)
0.80	$U_{0.20}La_{0.80}O_{1.80}$	0.56360(2)

precursor procedure. Stoichiometric amounts of lanthanum uranyl propionate and lanthanum sesquioxide (previously calcined at 900°C) were pyrolized at 750°C, before being fired in air at the temperatures indicated in Table 1, and then quenched to room temperature by rapidly removing them from the furnace. Samples quenched from 1400°C were in addition annealed at 1100°C for 500 hr and quenched to room temperature. Uranium and lanthanum were quantitatively determined by inducted coupled plasma (ICP) with a Perkin–Elmer Plasma 40 emission spectrometer. Oxygen content was determined by a backcerimetric titration method (21, 22).

X-ray powder diffraction patterns were recorded on a Siemens D-501 diffractometer with monochromatized CuK_α radiation. Diagrams were recorded in the step-scanning mode, at 0.02° 2θ step scanning and 5 sec counting time. Indexing of powder patterns of annealed samples was obtained using the program Treor-4 (23).

Electron diffraction and microscopy were carried out on JEOL 2000 FX and JEOL 4000 EX electron microscopes, fitted with double tilting goniometer stages of ±45° and ±25° respectively. Specimens were crushed and dispersed in acetone and then transferred to holey carbon-coated copper grids.

RESULTS

All specimens were obtained as orange powders suggesting that the uranium ions in the specimens are in the hexavalent state. Determination of uranium and lanthanum indicates that there was no appreciable volatilization of the metallic elements during sample preparation. The oxygen content determination carried out for single phase materials indicates that all of them are oxygen defficient, and all the uranium ions in the solid solutions are in the hexavalent state. Table 2 lists the fluorite-type solid solutions $(U_{1-y}La_y)O_{2-x}$, their experimental compositions deduced from chemical analysis and their lattice parameters.

X-ray powder diffraction patterns recorded on materials quenched from 1400°C indicate that they are single phase compounds having the fluorite-type structure over the whole compositional range. The cell parameter a increases linearly with increasing the La content (y) in the oxides, as shown in Table 2. A representative pattern recorded on sample $U_{0.26}La_{0.74}O_{1.89}$ is presented in Fig. 1a.

X-ray patterns recorded on materials with compositions $y = 0.73$ and $y = 0.74$ either obtained or annealed at 1100°C are alike. In Fig. 1b, the diagram for sample $U_{0.26}La_{0.74}O_{1.89}$ is depicted. This pattern is fairly similar to the one reported by Diehl and Keller for the phase 75% $LaO_{1.5}$, 25% UO_3 at 1100°C (17). These authors indexed the diagram by analogy to the R_I phase (UY_6O_{12}) (24, 25), on the basis of an hexagonal–rhombohedral cell, with parameters $a_h = 1.036$ nm, $c_h = 0.9987$ nm (18). However, from a closer inspection of both patterns, some nonnegligible differences arise and the indexing of the powder pattern obtained in this work suggests an hexagonal cell with parameters $a_h = 0.78220(4)$ nm and $c_h = 0.99712(7)$

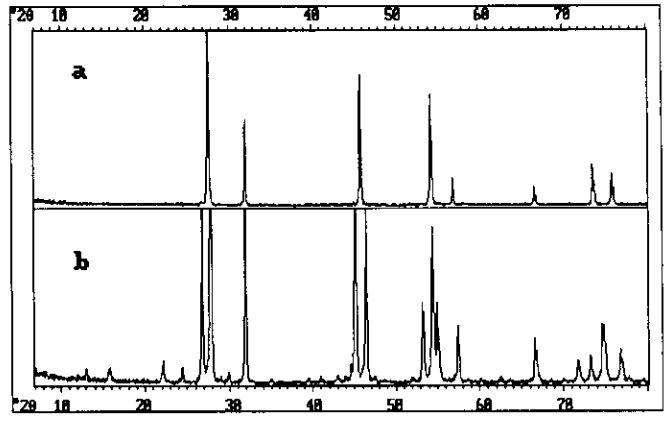

FIG. 1. X-ray powder diffraction patterns of the material $U_{0.26}La_{0.74}O_{1.89}$: (a) quenched from 1400°C, (b) annealed at 1100°C for 500 hr.

TABLE 3
X-Ray Powder Diffraction Data for $U_{0.26}La_{0.74}O_{1.89}$ Annealed at 1100°C

$h\ k\ l$	$2\theta_{Obs}$	$2\theta_{Calc}$	d_{Obs}	I/I_0
1 0 0	13.047	13.059	0.6780	2.4
1 0 1	15.807	15.803	0.5602	2.8
1 0 2	22.111	22.120	0.4017	3.2
1 1 1	24.421	24.428	0.3642	2.6
0 0 3	26.799	26.801	0.3324	34.2
2 0 1	27.805	27.795	0.3206	100.0
1 1 2	28.995	28.994	0.3077	1.1
1 0 3	29.910	29.921	0.2985	1.5
2 0 2	31.925	31.917	0.2801	44.5
2 1 0	35.023	35.018	0.2560	0.9
2 1 2	39.546	39.536	0.2277	1.2
3 0 1	40.952	40.947	0.2202	1.0
1 1 4	42.995	42.993	0.2102	1.5
3 0 2	44.006	43.986	0.2056	1.0
2 1 3	44.647	44.639	0.2028	1.3
2 0 4	45.116	45.123	0.2008	26.2
2 2 0	46.409	46.396	0.1955	25.7
1 0 5	47.490	47.488	0.1913	1.0
3 1 2	51.974	51.971	0.1758	1.1
2 0 5	53.278	53.262	0.1718	10.8
2 2 3	54.407	54.391	0.1685	20.6
4 0 1	54.936	54.950	0.1670	11.8
4 0 2	57.441	57.420	0.1603	7.0
2 1 5	58.642	58.629	0.1573	0.9
3 2 1	60.241	60.218	0.1535	0.9
3 2 2	62.540	62.555	0.1484	1.0
4 1 1	63.590	63.578	0.1462	0.7
4 0 4	66.709	66.718	0.1401	5.7
3 1 5	68.596	68.567	0.1367	0.7
3 0 6	70.238	70.271	0.1339	0.7
1 1 7		70.272		
2 0 7	71.842	71.839	0.1313	3.1
4 0 5	73.263	73.272	0.1291	3.3
4 2 1	74.679	74.695	0.1270	7.6
2 2 6	74.955	74.931	0.1266	8.0
4 2 2	76.809	76.806	0.1234	4.8
3 2 5	77.850	77.863	0.1226	0.8
1 0 8		77.864		
3 0 7	79.472	79.491	0.1205	0.8

Note. Unit cell parameters, $a_h = 0.78220(4)$ nm, $c_h = 0.99712(7)$ nm. Unit cell volume = 0.52835 nm^3.

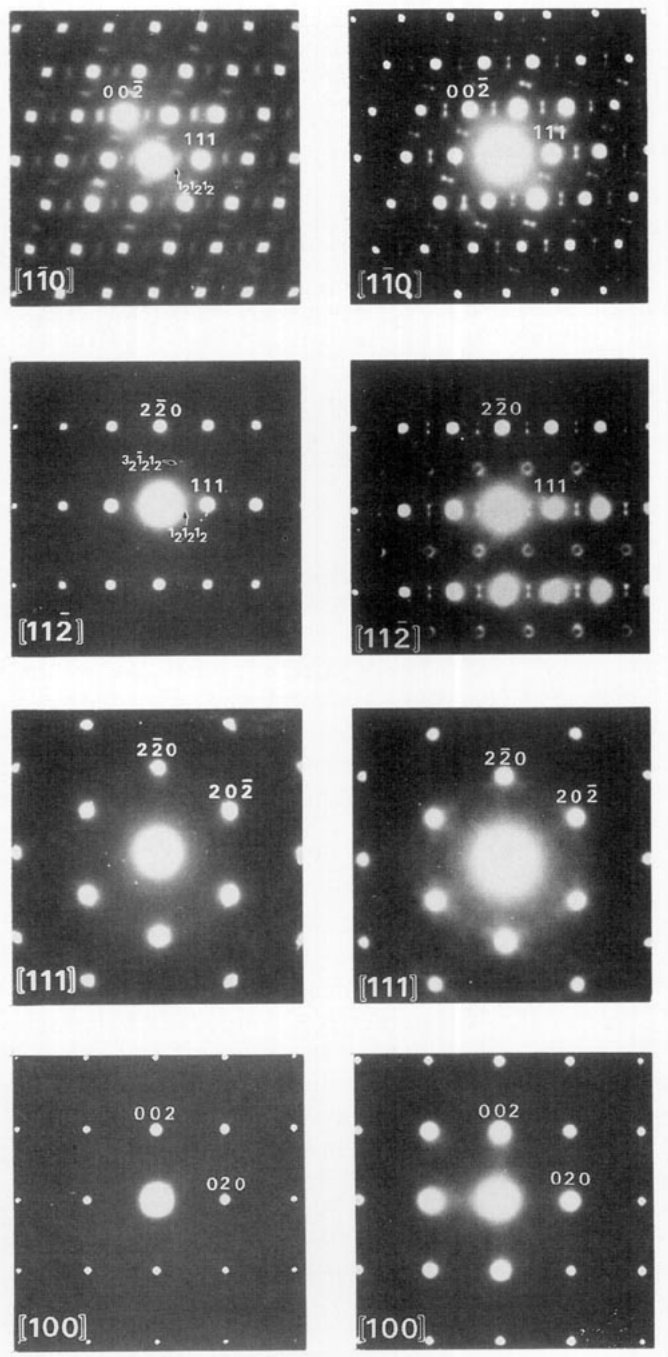

FIG. 2. Electron diffraction patterns for materials $U_{0.26}La_{0.74}O_{1.89}$ (left) and $U_{0.20}La_{0.80}O_{1.80}$ (right) quenched from 1400°C.

nm. Powder diffraction data for this material are given in Table 3.

Representative selected area electron diffraction patterns for samples $U_{0.26}La_{0.74}O_{1.89}$ and $U_{0.20}La_{0.80}O_{1.80}$ quenched from 1400°C are presented in Fig. 2, along the $[1\bar{1}0]_c$, $[11\bar{2}]_c$, $[111]_c$, and $[100]_c$ orientations of the cubic fluorite cell. In all cases, there is a set of strong Bragg reflections consistent with a fluorite-type (space group $Fm3m$) average structure. In addition, a characteristic diffuse intensity distribution, situated at $\approx \frac{1}{2}\langle 111\rangle_c^*$ is particularly apparent in the $[1\bar{1}0]_c$ and $[11\bar{2}]_c$ zone axes patterns. In the $[11\bar{2}]_c$ zone axis, "smoke-rings" diffuse maxima at $\approx \frac{1}{2}\langle 3\bar{1}1\rangle_c^*$ are also present. The similarity between the diagrams of both materials is evident and a somewhat better resolution of the diffuse maxima in sample $y = 0.80$ is appreciable.

Lattice images along the $[1\bar{1}0]_c$and $[11\bar{2}]_c$ zone axes of sample $y = 0.74$, are shown in Fig. 3. Zones with regular

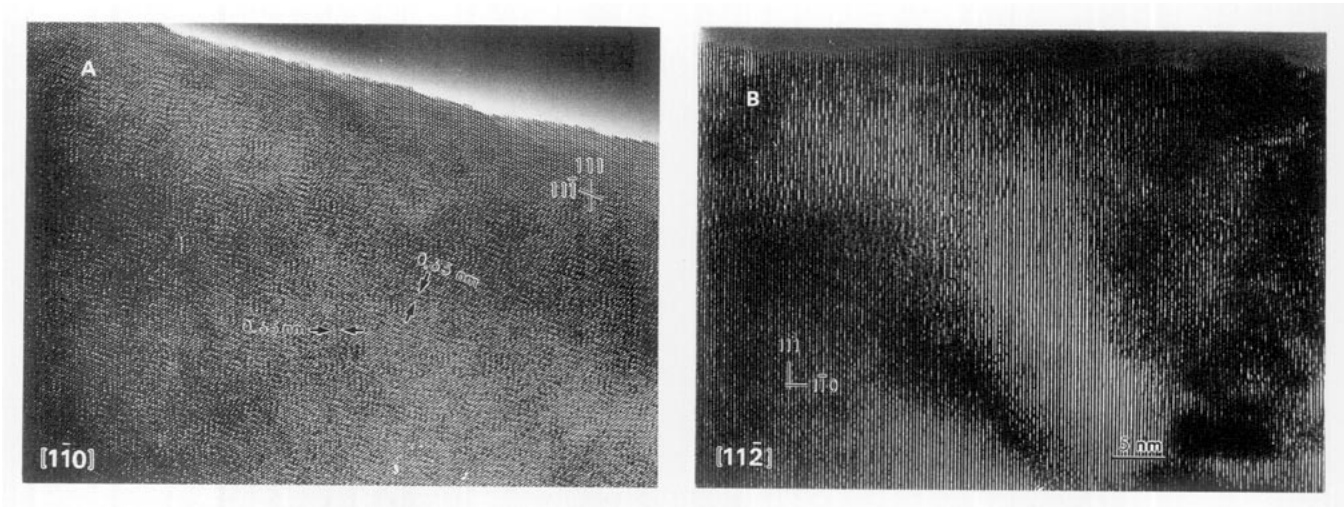

FIG. 3. High resolution images of the material $U_{0.26}La_{0.74}O_{1.89}$ quenched from 1400°C: (A) along $[1\bar{1}0]_c$ and (B) along $[11\bar{2}]_c$ zone axes.

fringes corresponding to the fluorite structure coexist with regions in which irregular features in contrast are evident. In Fig. 3a, zone axis $[1\bar{1}0]_c$, distances of 0.65 nm corresponding to $\approx 2 \times d_{(111)c}$ are randomly distributed throughout the fluorite matrix. Figure 3b, along the $[11\bar{2}]_c$ zone axis, shows modulations of contrast in the fluorite planes.

Patterns obtained for $U_{0.26}La_{0.74}O_{1.89}$ annealed at 1100°C are presented in Fig. 4, along the same orientations as in the previous case. The presence of $(00l)_h^*$ reflections confirms that the structure of the R_{II} phase does not fulfill the extinction conditions for a hexagonal–rhombohedral cell, and subsequently it must be described on the basis of a hexagonal–primitive cell, as the one deduced from X-ray diffraction data. Morevoer, these diagrams deserve further comments. Diffuse scattering has vanished, and two sets of medium and low intensity superstructure spots are found at positions corresponding to the R_{II} structure. They are located in between a set of stronger reflections that are still consistent with the fluorite type structure. The scheme depicted in Fig. 5 accounts for the relationship between the diffuse intensity in the high-temperature samples and sharp satellite spots in annealed materials. According to this, the streaking of the diffuse spots could be originated by the overlapping of the two most intense superstructure maxima. In the high-temperature material, as microdomains are randomly distributed, diffuse maxima appears along the $\langle 111\rangle_c^*$fluorite directions. However, when the R_{II} phase exists as a single phase, the symmetry is lowered, the equivalence of the $\langle 111\rangle_c$ directions is no longer maintained, and therefore, the two most intense superstructure spots only appear along one of the $\langle 111\rangle_c^*$directions.

In Fig. 6, a structural image along the $[100]_h \parallel [1\bar{1}0]_c$ zone axis is shown. Fringes with interplanar spacings $d_{(001)} = 0.99$ nm and $d_{(010)} = 0.68$ nm are easily recognized and confirm the proposed new cell.

Furthermore, although the X-ray pattern indicates that this material is a single phase, in Fig. 6, regions with interplanar spacings of 1.36 nm $\approx 2 \times d_{(010)h}$ alternate in a disordered fashion with fringes of the R_{II} phase. This can be interpreted as isolated layers of an $n = 2$ superstructure of the R_{II} cell "inserted" into the basic hexagonal structure, as confirmed by the corresponding Fourier transform.

The relationships between the cubic fluorite and the hexagonal R_{II} cell can be established from the corresponding electron diffraction patterns along the zone axes $[100]_h \parallel [1\bar{1}0]_c$ and $[001]_h \parallel [111]_c$, (Figs. 2 and 4):

$$\mathbf{a}_h^* = \tfrac{1}{6}[4\bar{2}\bar{2}]_c^*$$

$$\mathbf{b}_h^* = \tfrac{1}{6}[22\bar{4}]_c^* \qquad [1]$$

$$\mathbf{c}_h^* = \tfrac{1}{3}[111]_c^*;$$

$$\begin{bmatrix} a \\ b \\ c \end{bmatrix}_h^* = \begin{bmatrix} \frac{4}{6} & -\frac{2}{6} & -\frac{2}{6} \\ \frac{2}{6} & \frac{2}{6} & -\frac{4}{6} \\ \frac{1}{3} & \frac{1}{3} & \frac{1}{3} \end{bmatrix} \begin{bmatrix} a \\ b \\ c \end{bmatrix}_c^* \qquad [2]$$

and in the real space:

$$\begin{bmatrix} a \\ b \\ c \end{bmatrix}_h = \begin{bmatrix} 1 & -1 & 0 \\ 0 & 1 & 1 \\ 1 & 1 & 1 \end{bmatrix} \begin{bmatrix} a \\ b \\ c \end{bmatrix}_c. \qquad [3]$$

From the above indicated expressions, the cell parameters of the R_{II} phase in the composition range $0.72 < y < 0.75$ can be related to the cubic parent structure as follows:

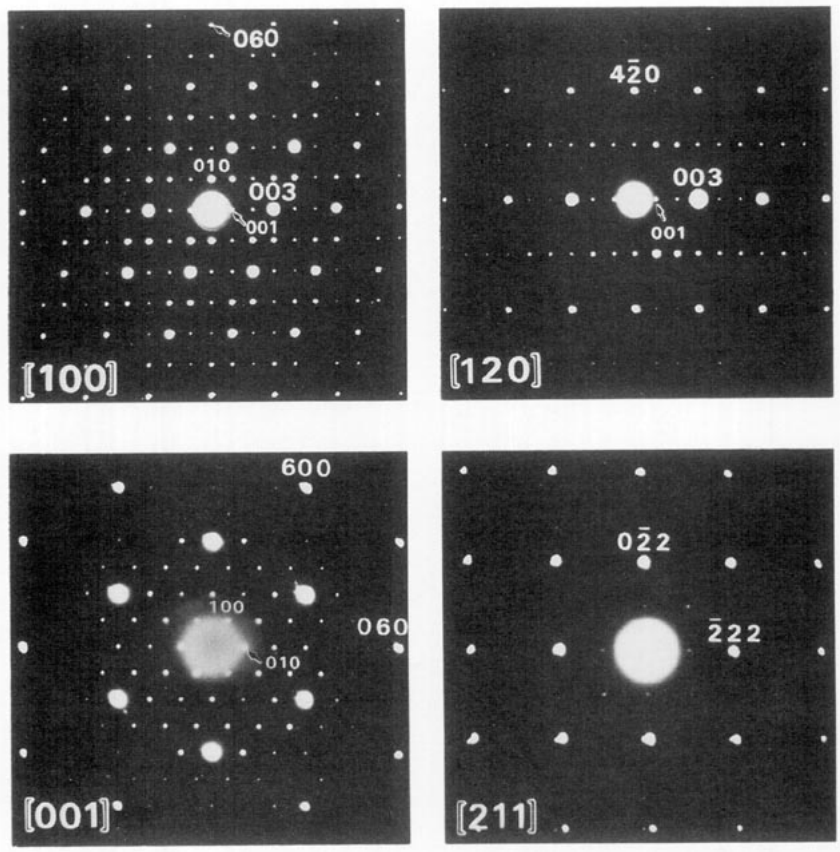

FIG. 4. Electron diffraction patterns of the material $U_{0.26}La_{0.74}O_{1.89}$ annealed at 1100°C. Hexagonal zone axes are indicated.

$$\begin{aligned} \mathbf{a}_h &= \mathbf{a}_c - \mathbf{b}_c & a_h &= \sqrt{2}a_c \\ \mathbf{b}_h &= \mathbf{b}_c - \mathbf{c}_c & b_h &= \sqrt{2}a_c \\ \mathbf{c}_h &= \mathbf{a}_c + \mathbf{b}_c + \mathbf{c}_c & c_h &= \sqrt{3}a_c . \end{aligned} \qquad [4]$$

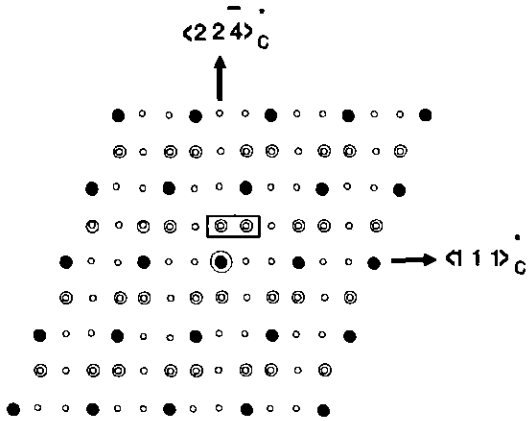

FIG. 5. Schematic representation of the electron diffraction pattern shown in Fig. 4 along the $[100]_h$ zone axis. It accounts for the relationship between diffuse intensity and sharp satellites spots in high and low temperature materials respectively.

Figure 7 schematizes the relationship between the hexagonal and cubic cells in reciprocal and real space.

DISCUSSION

Mixed oxides $(U_{1-y}La_y)O_{2-x}$ formed in the compositional range $0.70 \leq y \leq 0.80$ at 1400°C in air crystallize,

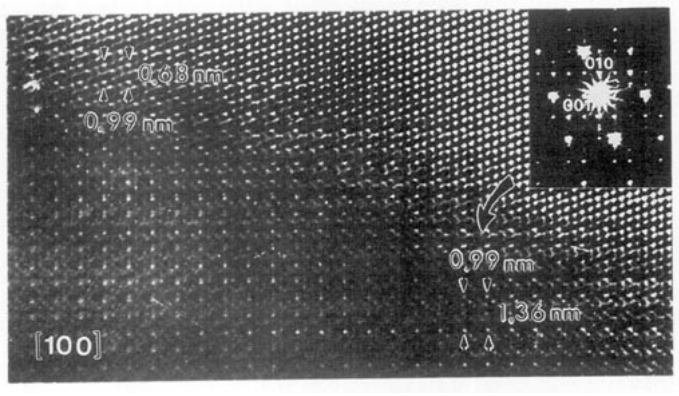

FIG. 6. Structure image corresponding to the material $U_{0.26}La_{0.74}O_{1.89}$ annealed at 1100°C, along the $[100]_h$ zone axis. Fringes corresponding to the R_{II} phase and R_{II} superstructure are indicated. The corresponding Fourier transform is shown in the inset.

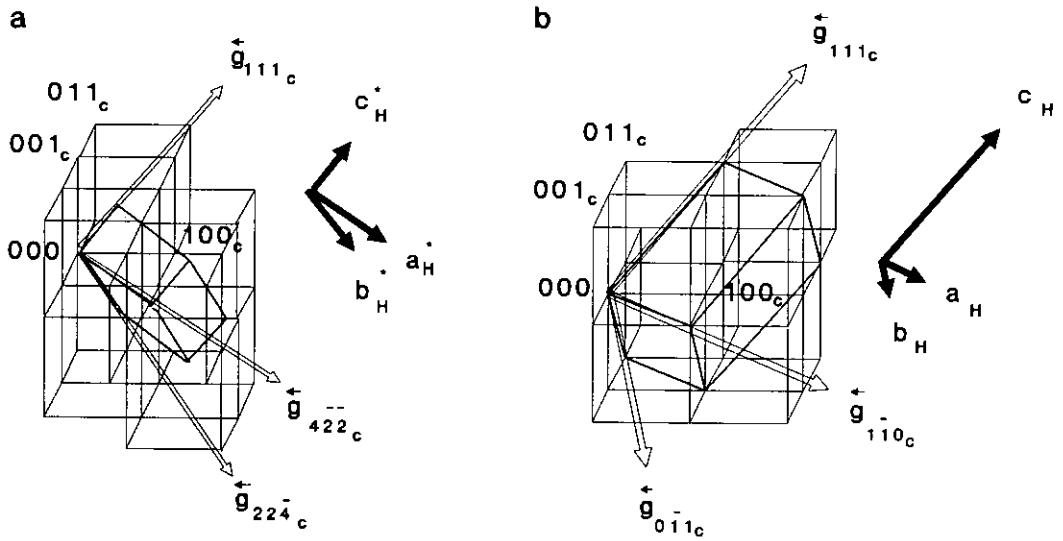

FIG. 7. Schematic representation of the R_{II} hexagonal lattice showing the relative orientations with respect to the cubic fluorite cell: (a) reciprocal space, (b) real space.

according to the X-ray powder data, in the fluorite-type structure, space group $Fm3m$. However, electron microscopic results indicate that full randomization of the cation sublattice has not been attained. Instead, the materials contain domains or nuclei with a partial cation ordering that it is closely related to the cation distribution found in the ordered R_{II} phase formed upon annealing at 1100°C.

Because cation mobility in this and other related systems is very low (26), this degree of heterogeneity will not be changed significantly except by annealing for long periods and complete equilibrium is only attainable under these conditions. In fact, the R_{II} phase is only obtained after annealing for at least 500 hr at 1100°C.

X-ray and electron microscopy data obtained on high- and low-temperature materials make evident the close relationship between the fluorite parent structure and the R_{II} phase formed in the compositional range $(U_{1-y}La_y)O_{2-x}$ $0.72 < y < 0.75$. The latter can be described as a superstructure of the fluorite cell, with two sixfold superlattices along the $[4\bar{2}\bar{2}]_c^*$ and $[22\bar{4}]_c^*$ and a threefold superlattice along the $[111]_c^*$.

It can be inferred that the ordered R_{II} phase crystallizes in the trigonal system in a primitive cell and lattice parameters determined for the material with composition $y = 0.74$ are $a_h = 0.78220(4)$ nm and $c_h = 0.99712(7)$ nm.

On the other hand, the presence of isolated layers of a probable $n = 2$ superstructure of the R_{II} phase suggests an ordering of the vacancies in the anion sublattice rather than a rearrangement of the cation sublattice. However, current available data do not permit to discriminate between both options. The analysis of HREM images in both R_{II} and R_{II} superstructure are now in progress, which will permit to outline a model for the anion vacancy distribution and for the heavy atoms positions, in order to solve both structures by the Rietveld method from X-ray and neutron diffraction data.

The calculated cell parameter values for the R_{II} phase are closely related to those determined for the R_{III} phase, formed in the same system in the interval $0.56 \leq y \leq 0.67$, (12, 18, 19), being $a_{RII} \approx 2 \cdot a_{hRIII}$ and $c_{RII} \approx c_{hRIII}/2$. It suggests a close relationship between the crystal structures of these two "ordered phases" formed in the U–La–O system.

ACKNOWLEDGMENTS

We thank Professor F. Hernández-Cano for his valuable comments. We acknowledge Mr. A. Garcia-Delgado for performance of the electron microscopy investigations and Mr. R. Ropero for technical assistance. We also express our gratitude to the Centro de Microscopía Electrónica of the Universidad Complutense de Madrid for facilities with HREM. This work has been supported by the CICYT project MAT 89–0567.

REFERENCES

1. Y. Arai, T. Ohmichi, S. Fukushima, and M. Handa, *J. Nucl. Mater.* **150,** 233 (1987).
2. T. B. Lindemer and A. L. Sutton, Jr., *J. Am. Ceram. Soc.* **71,** 553 (1988).
3. T. Fujino, T. Yamashita, and H. Tagawa, *J. Solid State Chem.* **73,** 544 (1988).
4. A. C. Monin, E. B. Mirza, and M. D. Mathews, *J. Nucl. Mater.* **185,** 308 (1991).
5. Y. Hinatsu, *J. Solid State Chem.* **94,** 163 (1991).
6. T. Fujino, T. Yamashita, and K. Ouchi, *J. Nucl. Mater.* **183,** 446 (1991).
7. Y. Hinatsu, *J. Solid State Chem.* **95,** 300 (1991).

8. R. J. Ball, *J. Mater. Chem.* **2,** 641 (1992).
9. S. P. S. Badwall, F. T. Ciacchi, and D. K. Sood, *J. Mater. Sci.* **21,** 4035 (1986).
10. M. P. van Dijk, F. C. Mijlhoff, and A. J. Burggraaf, *J. Solid State Chem.* **62,** 377 (1986).
11. P. Herrero and R. M. Rojas, *J. Solid State Chem.* **73,** 536 (1988).
12. P. Herrero, P. Garcia-Chain, and R. M. Rojas, *J. Solid State Chem.* **87,** 331 (1990).
13. M. C. Pienkowski, M. L. Jenkins, and P. T. Moseley, *J. Solid State Chem.* **92,** 543 (1991).
14. R. Wallenberg, R. L. Withers, D. J. M. Bevan, J. G. Thompson, P. Barlow, and B. G. Hyde, *J. Less-Common Metals* **156,** 1 (1989).
15. R. L. Withers, J. G. Thompson, and P. Barlow, *J. Solid State Chem.* **94,** 89 (1991).
16. R. L. Withers, J. G. Thompson, P. Barlow, and J. C. Barry, *Aust. J. Chem.* **45,** 1375 (1992).
17. H. G. Diehl and C. Keller, *J. Solid State Chem.* **3,** 621 (1971).
18. C. Keller, "Gmelin's Hanbuch der Anorganischen Chemie," System-Nr55, U, Teil C, pp. 213–221. Springer-Verlag, Berlin/New York, 1975.
19. R. M. Rojas, P. Garcia-Chain, and P. Herrero, *Solid State Ionics* **44,** 263 (1991).
20. G. G. Koshecheev, L. M. Kovba, and V. I. Spytsyn, *Dokl. Akad. Nauk SSSR* **175,** 92 (1967).
21. S. R. Dharwadkar and M. S. Chandrasekharaiah, *Anal. Chim. Acta* **45,** 545 (1969).
22. T. Fujino and T. Yamashita, *Fresenius Z. Anal. Chem.* **314,** 156 (1983).
23. P. E. Werner, Program Treor-4, University of Stockholm, S-10691 Stockholm, 1984.
24. E. A. Aitken, S. F. Bartram, and E. F. Juenke, *Inorg. Chem.* **3,** 949 (1964).
25. Y. Hitnasu, N. Masaki, and T. Fujino, *J. Solid State Chem.* **73,** 567 (1988).
26. D. J. M. Bevan and E. Summerville, *in* "Handbook of the Physics and Chemistry of Rare Earth" (K. A. Gschneider, Jr., and L. Eyring Eds.), Vol. 3, p. 437. North-Holland, Amsterdam, 1984.